

Copyright © 1982, by the author(s).
All rights reserved.

Permission to make digital or hard copies of all or part of this work for personal or classroom use is granted without fee provided that copies are not made or distributed for profit or commercial advantage and that copies bear this notice and the full citation on the first page. To copy otherwise, to republish, to post on servers or to redistribute to lists, requires prior specific permission.

EXPERIMENTAL STUDY OF HIGH β BALLOONING MODES

by

H.D. Price, N.M.P. Benjamin, A.J. Lichtenberg and M.A. Lieberman

Memorandum No. UCB/ERL M82/54

June 1982

ELECTRONICS RESEARCH LABORATORY

College of Engineering
University of California, Berkeley
94720

Experimental Study of High β Ballooning Modes

by

H.D. Price, N.M.P Benjamin, A.J. Lichtenberg and M.A. Lieberman

Department of Electrical Engineering and Computer Sciences
and the Electronics Research Laboratory
University of California, Berkeley, CA 94704

ABSTRACT

Ballooning instabilities have been studied in the Berkeley Multiple Mirror Experiment. Counter-streaming theta pinch and Marshall gun source plasmas have been used to achieve a high β (>20 percent) at a sufficiently high temperature ($T_e = T_i \approx 15$ eV). Four different field configurations were investigated, each at varying mirror ratios, to explore a range of drive and connection length parameters. In two of these the magnetic field was pulsed to obtain a locally unstable configuration for initiation of ballooning activity. The other two configurations were a weakly unstable local field region, and the standard multiple-mirror configuration. The results were compared with theoretical predictions from a high m-number Livermore ballooning code.

In general, the experimental plasma was found to be absolutely more stable than predicted by MHD flute or ballooning theory, possibly due to effects such as additional inertia in the end solenoidal regions, wall stabilization, and FLR stabilization of the theoretically most unstable high m-number modes. The criterion used experimentally for determining the existence of a ballooning mode was a consistent ratio greater than 1.5 in mode amplitude between the unstable and stable regions. These

* Report prepared for the Department of Energy under Contract DE AT03 76ET5039.

results were compared with two theoretical calculations. In the first, we assumed free (floating) mode amplitude boundary conditions at the ends of the device, with the existence of ballooning indicated by the same ratio of 1.5. In the second, we assumed zero mode amplitude boundary conditions with the existence of ballooning indicated by the transition to instability. Both criteria are considered (see sec. IV) to give upper bounds on experimental values of β_c . Depending on the configuration, a β of 5-15 percent was found experimentally to result in ballooning instability. These values were generally somewhat lower than those predicted by either of the theoretical models, in agreement with expectations.

I. Introduction

Ballooning instabilities may be of great importance in both linear and toroidal confinement schemes. In shearless minimum average B, linear systems, such as multiple mirror and tandem mirror devices, the critical β for ballooning may set severe limits on engineering and economic feasibility of reactors. The presence of shear and closed magnetic surfaces in toroidal systems complicates the analysis of ballooning modes. With these effects absent in linear systems, analysis is simplified and comparison with experiments facilitated. Ballooning mode stability is a concern for multiple mirror confinement. The ten meter multiple mirror at Berkeley⁽¹⁾ is designed to be stable to ballooning modes in the mirror throats up to $\beta \sim 1$, using approximate stability criterion:⁽²⁾

$$\beta_c \leq \frac{8\pi^2 \gamma r_p R_c}{\ell_m^2}$$

where γ is the ratio of average good curvature to the maximum destabilizing curvature R_c , r_p is the plasma radius, and ℓ_m is the connection length. For the ten meter device we have calculated $\gamma \sim 0.1 \ell_m / \ell_c$ and $R_c \sim \ell_c \ell_m / r_p$, where $\ell_c =$ cell length, which yields $\beta_c \leq 8$. Furthermore, the region of bad curvature occurs where the field is a maximum, and consequently where β is a minimum.

Ballooning in tandem mirrors is theoretically a more severe problem, as the bad curvature occurs in a weak field region, and the connection lengths are long. Extensive analyses of tandem mirror

configurations have been made at the Lawrence Livermore National Laboratory, using numerical codes employing an ideal MHD model in the short wavelength (high m-number) limit.^(3,4) Typical results obtained from these codes suggest that stable central cell β 's greater than 20 percent are difficult to achieve. However, it is well known that high-m modes, which are theoretically most unstable in the MHD limit, are actually stabilized by finite-Larmor-radius (FLR) effects. The $m = 1$ (displacement mode) may be the most dangerous; the experimentally observed instabilities we report here do, in fact, have primarily an $m = 1$ component.

At very high β 's, ballooning can occur in multiple mirrors or in tandem mirrors in a neutral or weakly good curvature field due to the finite plasma pressure and resulting "diamagnetic" expansion of the field lines. An estimate of the curvature reversal can be obtained from the equilibrium equations in a long, thin mirror cell:

$$p + B^2/2\mu_0 = B_v^2/2\mu_0, \quad Q = Q_v$$

where p is the plasma pressure, Q is the fan ellipticity, and the subscript "v" denotes vacuum ($\beta=0$) quantities. These equations, along with flux conservation and the condition of constant pressure along a field line, determine the field line equation $r(z)$ as a function of the midplane β . In the ten meter device for optimum setting of the strong and weak quadrupole currents, $\beta \sim 0.4$ for reversal of curvature in the midplane. (For collisionless equilibria, such as the tandem mirror, the pressure is anisotropic and the field line equation and curvature reversal condition are considerably more difficult to obtain from the self-consistent equilibrium.) This effect can be investigated in the standard multiple-mirror configuration. With quadrupole currents set for fully stabilization this

unstable behavior was not observed; although the plasma appeared to be somewhat less stable at the highest values of β ($\beta > 25\%$) with some movement observed on occasional shots.

The primary purpose of this investigation is to determine if the high m number ballooning codes adequately predict the ballooning activity observed in a number of experimental magnetic field configurations in the ten meter device. To do this we wish to have ballooning activity at reasonably low values of β . It is therefore necessary to modify the multiple mirror magnetic fields to increase the curvature drive and the connection lengths, while still maintaining flute stability.

To experimentally investigate ballooning modes in the ten meter device, we have employed three techniques. (1) We have continuously varied the quadrupole field current to weaken and reverse the good curvature region in the midplane region of each cell. (2) We have modified the vacuum curvature in two adjacent cells near the θ -pinch end of the device, by removing the weak quadrupole current in those cells while maintaining favorable curvature in the cells bounding this region. (3) We have changed the field configuration transiently by pulsing on a fast rising field to cancel the quadrupole fields in some sections of the device. Alternatively the field shape was modified to give a locally unstable field region, by transiently pulsing on mirrors in a solenoidal region. Three different pulsed configurations have been investigated to give varying connection lengths, each with varying mirror ratios to produce varying drives.

A major difficulty has been to achieve the initial plasma conditions that are necessary to clearly observe ballooning mode activity. In preliminary experiments a drifting plasma was injected by a theta-pinch source located at one end of the ten meter device. The plasma behavior

was monitored by Langmuir probe arrays located at several axial positions. The fields (midplane strength: $B_0 \sim 1.4$ kG) were locally destabilized by removing all weak quadrupole contributions in two adjacent cells. Low azimuthal mode number (primarily $m = 1$) instabilities were observed. There were discernable differences (in the axial structure) between these modes and those obtained by removing the weak quadrupole currents globally. These differences were interpreted as "quasi-ballooning" effects and will be discussed in section IV.

There were several experimental shortcomings. The plasma had a large flow velocity compared to its thermal velocity during the experiment, and it was injected into an unstable field configuration. Thus it was not possible to properly study the behavior of an equilibrium with respect to small perturbations, since growth was convective and proceeded while the plasma was still transient. The obtainable values of β ($>20\%$) in the central field region were sufficient to produce instabilities but with the fairly modest values of ion temperatures ($T_i \approx 5$ eV) the predicted growth rates were quite close to the density decay time constant at peak β ($\gamma \sim 20$ μ sec). For these reasons it became desirable to reduce the flow and to thermalize some portion of the drift energy.

A second source, employing a Marshall gun installed at the opposite end of the device to the θ -pinch, proved to be versatile and quite effective in greatly reducing the flow velocity. Mean free paths near the leading edges of the two injected plasmas were long, so that the two colliding plasmas mixed and interacted over several cell lengths. The thermalization produced peak temperatures exceeding 15 eV with peak (on axis) beta values in the interaction zone of over 30%. However the expected enhancement of the confinement (due to the reduction of the

drift) was offset by an increase in the severity of the radial loss at higher temperatures. In order to maximize the confinement time, the experiments we report here were performed at higher magnetic field strengths ($B_0 \approx 2$ kG) and lower than normal ellipticities. Under these circumstances the fields during injection were mildly unstable.

In general, the experimental plasma was found to be more stable than predicted by MHD flute or ballooning theory, possibly due to such effects as axially non-uniform pressure weighting and FLR stabilization. However, the ballooning character of the solutions at significant β generally agrees with theoretical predictions. The criterion used, experimentally, for determining the existence of a ballooning mode was that repeated shots in the experiment have at least a factor of 1.5 ratio in mode amplitude between the unstable and stable regions. This is the minimum easily resolvable mode difference. These experimental results were compared with two theoretical calculations. In the first, we assumed free (floating) mode amplitude boundary conditions at the ends of the device, with the existence of ballooning indicated by a factor of 1.5 change in mode amplitude from locally stable to unstable regions. In the second, we assumed zero mode amplitude boundary conditions with the existence of ballooning indicated by the transition to instability. (Also note that the observations are for a low azimuthal mode number, while the ballooning code uses a high m -number approximation). The results, are summarized below:

(i) With standard completely stabilized multiple mirror fields the plasma was stable at all measured values of β to $\beta > 25$ percent. This result is in agreement with MHD ballooning code theory which predicts ballooning stability up to $\beta = 1$, and a $\beta_c = .4$ for reversal of the midplane curvature. With weakened stabilizing fields (smaller weak quadrupole

currents) the plasma is more stable than either the MHD flute (MAFCO) or ballooning (Kaiser) codes would suggest. No ballooning is observed in the experimentally observed transition from stable to unstable behavior, but at the highest β 's the plasma is somewhat less stable.

(ii) With a weakly unstable region over two cells (weak drive and long connection length) the plasma was observed to balloon at β_c about 15 percent. The corresponding ballooning code (free boundary mode amplitude) predicted a factor of 1.5 mode amplitude difference at $\beta_c \approx 30$ percent.

(iii) The drive of the weakly unstable configuration (ii) was increased by pulsing on two magnetic mirrors. Experimentally, for moderate drive (mirror ratio $M = 3$) ballooning activity was observed to be initiated at $\beta_c \approx 10$ percent. Corresponding ballooning theory (free boundary mode amplitude) indicated a ballooning configuration at $\beta_c \sim 15$ percent. For this configuration the plasma was predicted to be flute unstable. With zero boundary mode amplitude the predicted transition to instability was at $\beta_c \approx 15$ percent. For stronger drive ($M = 4$) in these configurations the observed β for ballooning activity was $\beta_c \geq 5$ percent.

(iv) With two adjacent mirror cells pulsed unstable (symmetrically about a mirror throat), the experimental transition to ballooning activity was not observed for weak drive (mirror ratio $M = 3$). For strong drive ($M = 4$) ballooning activity occurred for $\beta_c \sim 10$ percent and for very strong drive ($M = 5$) ballooning occurred for $\beta_c \sim 7.5$ percent. Comparison with theory is more complicated in this case and will be reserved for a later section.

In Section II we describe the experimental apparatus and the diagnostics. In Section III the experimental results are given. In Section IV numerical results are presented and compared with the experiments.

II. The Experiment

A. Experimental configuration

The magnetic field consists of a one-meter guide field section and a series of mirror cells, as indicated in Fig. 1. The axial field consists of a uniform solenoid and nine sharp mirrors whose 75 cm spacing determines the cell length. Two sets of currents, a weak and a strong quadrupole, are present in each cell, and reverse polarities between cells. The quadrupole currents can be optimized to give the best minimum-average-B operation.⁽⁵⁾ The quadrupole components make the flux surfaces fan periodically in a series of ellipses with alternate vertical and horizontal major axes as seen in Fig. 2. The solenoidal, mirror, weak and strong quadrupole currents are provided by four separate capacitor banks, with the current rising in $\sim 500 \mu\text{s}$ and decaying $\sim 2 \text{ ms}$. For a mirror ratio $M = 4$, the optimal mirror throat ellipticity (major/minor radii) is ~ 24 ; for $M = 3$, the ellipticity is ~ 18 . In these experiments, the midplane magnetic field was operated between 1.4 and 2 kG which is approximately 35% of the maximum field allowed by the 300-kJ capacitor banks. These operating conditions were chosen as a compromise between the conflicting requirement of high β and low radial diffusion. The straight stainless-steel vacuum chamber has an inner diameter of 8.6 cm with a base pressure of $\leq 2 \times 10^{-6}$ Torr.

The main plasma source is a conical θ -pinch operated in either a ringing or crowbarred mode. Varying the gas pressure and timing from a puff value can vary the values of the plasma density and the plasma temperature. Varying the number of capacitors discharged into the θ -pinch also varies the total energy. At high densities most of the energy is converted to flow energy, so that increasing the ratio of peak θ -pinch field to multiple-mirror solenoidal field does not appreciably change the

plasma temperature in the multiple mirror. For the experiments in which the β is varied at a constant temperature, the density is generally controlled using a diaphragm aperture, located near the θ -pinch in the guide field, whose diameter can be continuously varied from 2 cm to 6 cm while under vacuum.

At low β (lower density and consequently long mean free path), efficient multiple-mirror trapping can be obtained with the single source. However at higher β the plasma is in a fluid flow regime in which only weak shocking in the mirror throats is available to stop the plasma flow from a single source.⁽⁶⁾ Consequently a second counter-streaming coaxial (Marshall) gun source was placed at the other end of the device. Some of the mirror and quadrupole coils were not energized in order that injection from the Marshall gun was also into a solenoidal field. The filling pressure and gun voltages were varied to approximately match the energy of the plasma produced by the Marshall gun to that produced by the θ -pinch in the main multiple-mirror interaction region.

B. Diagnostics

The experimental data is obtained with Langmuir probes (density and plasma radius), a triple-probe (density and temperature), compensated diamagnetic loops (beta and temperature), and a plasma camera (plasma cross-sections). A set of four Langmuir probes arrayed azimuthally at a single midplane is used to follow the plasma motion in time. Assuming a given mode structure, the measurements are analyzed to yield the transverse motion of the center of the plasma cross-sectional density distribution.

An accurate measurement of the plasma β is required for comparison with numerical prediction of the critical β for ballooning. The theory

uses an on-axis β together with a Gaussian radial distribution. The diamagnetic loops on the other hand, measure an average β over a given plasma area. Time dependent radial profiles are required to convert this data into that required for the theory. The profiles were found to be more flat-topped than Gaussian, and it is estimated that errors of the order of 20 percent can be introduced through the use of an assumed Gaussian profile matched to the measured plasma profile.

The triple-probe was very useful in obtaining a time resolved electron temperature. The temperature was compared to that obtained at a single time from a set of static measurements on a single Langmuir probe and found to be in good agreement. The contribution of drift to Langmuir probe and triple-probe current is approximated by the expression $I = \sqrt{I_i^2 + I_d^2}$, where I_i is the thermal ion saturation current given by Laframboise, and $I_d \equiv nevA'_p$, where A'_p is the projected probe area in the direction of flow. The density found from a single Langmuir probe or from the triple probe (used as a double probe) was within 20 percent of the density obtained from the combination of on-axis β and triple probe temperature measurements.

Plasma camera pictures were useful in identifying mode structures but had to be used with care when interpreting the density profile of the plasma. The optical lens system for the plasma camera captures some spurious light which is presumably scattered from the internal structure of the camera. This appears on the photograph as a halo that outlines the excited regions and adds to the already diffuse nature of the plasma pictures. The camera pictures have been compared with data from a Langmuir probe array positioned near the front face, and the two measurements show qualitative agreement. Differences in relative

brightness (on a given shot) may be interpreted as corresponding qualitative density differences.

III. Experimental Results

A. Preliminary experiments with a single source

In the first experiment, plasma was injected from the θ -pinch into the stabilized multiple-mirror fields with the diaphragm wide open. Peak β values above 40 percent were observed. The position of peak density convected through the cells with indication of both trapping and radial loss. The plasma decayed stably, as seen in Fig. 3 showing both probe traces in mirror cells 3 and 4 (M_{23} and M_{34}) and an end-on picture of the plasma taken with a plasma camera, which terminates the plasma at a time (~ 120 μ sec after the θ -pinch is fired) in cell⁽⁵⁾ (M_{45}). The experiments were repeated with an axial probe array and the resulting decay is plotted in Fig. 4. In these experiments the mirror ratio was 3. The decay rates were compared with classical radial loss rates (enhanced by the fan ellipticity) under two sets of assumptions as to loss processes.⁽⁷⁾ The experimental results agree reasonably well with the theory, indicating the classical nature of the loss.

The results in Fig. 3 are contrasted to those in Fig. 5 in which the plasma is injected into an unstable field configuration (no weak quadrupoles). The plasma is convectively unstable with large amplitude radial displacements already apparent at the midplane of the first observation cell (M_{23} = cell 3). Because the temperature falls during the pulse, the amplitude of the flute mode decays in time in a given cell, as a slower growing portion of the mode is convected into the cell. Thus, qualitatively the quasi-ballooning character of the mode is seen in the high β region of the pulse (near the leading edge) where the Alfvén velocity

is less than the plasma drift velocity ($V_A \leq V_D$); the centroid of the radial distribution is plotted against time in Fig. 5. The circles surrounding each plasma center give an indication of the uncertainty of the measurement of the center. A series of runs of this nature was performed with varying weak quadrupole field strength, indicating increasingly unstable behavior as the weak quadrupole strength was decreased below the optimum value. The plasma was calculated to be flute unstable (MAFCO)⁽⁸⁾ at all values for which unstable behavior was observed.

In a third experiment, the field was destabilized by removing the weak current quadrupole fields from two adjacent cells with midplanes M_{12} and M_{23} . The results are shown in Fig. 6 along with a sketch of the magnetic field line profiles in the stable and unstable region. The probe positions where the data was taken are noted. The plasma is seen to be unstable in the locally destabilized cells, with a partial restabilization in the downstream stable cell, a clear indication of a ballooning instability. The restabilization in time is again consistent with the interpretation that the mode is convected with the drift, with the later-arriving plasma being cooler and therefore growing more slowly. At an average $\beta \approx 20$ percent estimated for this experiment, the Alfvén velocity (at $T = 5$ eV) is $V_A \approx 6$ $\mu\text{sec cm}$ compared to the observed drift velocity $V_D \approx 5-8$ $\mu\text{sec cm}$, and thus the mode convects. The high m -number MHD code predicted an eigenfunction peaked in the unstable cell (see Fig. 15b next section).

For the unstable modes seen in Figs. 5 and 6 the four probe array gave only sufficient spatial resolution to track the motion of the plasma center. To supplement this information, a plasma camera was used to determine the m -number of the mode. The results of typical

plasma camera pictures are shown in Fig. 7. We note that the mode is primarily $m = 1$ (displacement) although some $m = 2$ and $m = 3$ activity is also seen. However, the $m = 1$ component is clearly the most dangerous for plasma loss, and thus tracking the center of the plasma distribution was considered adequate for diagnosing the instability. Although the plasma camera results only qualitatively determine the density profile, the center of the plasma may be determined with reasonable accuracy. As seen in Fig. 7, the camera pictures and probe plots (taken simultaneously) show good correlation, further justifying the use, of the probe array to track the unstable motion.

As discussed in the introduction, the interpretation of these results has been complicated by the effects of plasma flow and a plasma temperature which changes with time. The plasma flow at finite β (finite k_{\parallel} modes), combined with a plasma temperature that varies both in time and space, requires that the instability be studied in a frame fixed in the plasma, rather than in the machine. The resulting interpretation of the data as measured in the machine frame is considerably more complicated. In addition, there are some questions concerning the relation between the stability properties of flowing plasma and stationary plasma. Consequently, the flowing plasma experiments were not directly used to compare an experimental critical value of beta, β_c , with numerical codes. This comparison was made in a series of pulsed magnetic field destabilization experiments, in which counterstreaming sources were used, and the results are given in the following subsection.

B. Experiments with counterstreaming sources

A number of configurations were explored with counterstreaming plasma sources. The source strength and timing was adjusted such that the

interpenetrating streams mixed in the cells of interest. In this process drift energy was converted to random energy and the temperature typically rose by a factor of two or more, to between 15 and 20 eV.

In Fig. 8, results for the complete multiple mirror fields are presented. Typical values of β are shown in the cells and at the times of interest for the subsequent stability experiments. The relative uniformity of the β over these cells justifies use of a uniform β approximation in the theoretical comparisons. To the left of midplane M_{01} (cell 1) and to the right of midplane M_{45} (cell 5) there are long solenoidal regions containing considerable plasma which acts as an additional inertia that tends to line-tie the mode. These regions are implicitly considered in the theory, as described in Section IV.

In Fig. 9 for case i, with the full multiple mirror fields present in all cells, the probe traces and the corresponding center of the plasma is followed in time at midplanes M_{23} and M_{34} for the fully stabilized configuration. To increase the drive, a high mirror ratio ($M = 5$) is used. The plasma is seen to maintain its central position between the probes. These experiments were repeated over a range of β values up to $\beta \approx 25$ percent with similar stable decay seen in all cases.

In contrast, for the same mirror ratio, but no weak quadrupole fields (still case i) the plasma is seen in Fig. 10 to be continuously growing, with the center displaying both radial (outward) and azimuthal motion. As expected, the mode is essentially flutelike (the same radius and azimuthal values in adjacent cells). No significant effect with varying β has been observed for this highly unstable case. When the weak quadrupole current and β are both varied, there is a range of weak quadrupole currents for which unstable motion is sometimes, but not always, seen. In this current range there may be a weak β effect (more unstable at higher β)

but no consistent pattern was evident. All observed instability modes are flute-like. The corresponding (MAFCO) theory predicts the plasma to be $\int d\ell/B$ unstable in all instances for which unstable motion is observed.

Three configurations were explored in which ballooning was directly observed by locally modifying the fields in a region of the device. In the first configuration (case ii) the plasma is injected into a weakly unstable region in which both the destabilizing mirror fields and the stabilizing quadrupole fields have been removed. A sketch of the flux surfaces is given in Fig. 11a. The motion of the plasma centroid, together with the probe data from which it is obtained, is given in Fig. 11b. Note the clear ballooning character of the mode which is growing at M_{23} , a midplane with bad curvature, and is stable at M_{45} , a midplane with good curvature. Because of the weak drive and the fact that the worst bad curvature is relatively close to the good curvature region, the value of β at which ballooning is observed is relatively high, with $\beta_c \approx 15$ percent.

For this configuration, the drive was increased by pulsing on two magnetic mirrors within the solenoidal region (case iii). A sketch of the flux surface is shown in Fig. 12a. The bad curvature is both stronger and further removed from the region of good curvature. In Fig. 12b the characteristic motion of the plasma centroid is seen to have ballooning characteristics similar to that of the previous case. Here, for moderately increased drive ($M = 3$) the ballooning mode is observed with $\beta_c = 10$ percent. When the drive is increased by increasing the mirror ratio to $M = 4$, the ballooning was observed for β values above $\beta_c = 5$ percent. The third localized unstable configuration studied, corresponds to the flux surfaces shown in Fig. 6a. For this experiment (case iv) the plasma is injected into stable fields and the appropriate quadrupole

fields are transiently pulsed off to produce the unstable configuration. Unlike cases (ii) and (iii), the amount of unfavorable curvature is strongly dependent on the azimuthal direction, with the strongly unstable direction being vertical. The unstable midplanes are M_{12} and M_{23} . In Fig. 13 the rapid motion of the plasma centroid in the unstable direction is noted, together with the much stabler behavior at a midplane with good curvature, M_{34} . For this case the drive can be large but the connection length is shorter than in case (iii). Here, the plasma is found to be stable for weak drive (mirror ratio $M = 3$) up to the peak obtainable $\beta \sim 25$ percent. For stronger drive ($M = 4$) ballooning activity occurred for $\beta_c \geq 10$ percent and for very strong drive ($M = 5$) ballooning occurred for $\beta_c \geq 7.5$ percent.

IV. Comparison with theory

A computer code originally developed to investigate ballooning modes in tandem mirrors^(3,4) was modified to accommodate multiple mirror configurations. Since the symmetry breaking quadrupole field is weak compared to the main axisymmetric field, and because the radius of curvature of the main field is large compared with characteristic radial lengths, a paraxial approximation is made throughout. The finite β equilibrium used in the calculation includes a long-thin modification of the mod B surfaces and assumes no change in the equilibrium ellipticity from the vacuum fields. The pressure is taken to be isotropic and constant along the axis. The radial profile is Gaussian. The guiding center energy principle assumes a paraxial ordering.⁽⁹⁾ Hamilton's principle is used to derive an Euler-Lagrange equation for the perturbation, in the short perpendicular wavelength limit. For axisymmetric configurations, in the MHD approximation, the most unstable modes have the highest transverse

mode numbers. No such general result exists for quadrupole systems but the same dependence of stability on mode number is assumed. An eikonal representation of the transverse variation of the perturbed wave reduces the equation to Sturm-Liouville form (along any specified line) with eigenvalue ω^2 .

The code output includes axial plots of the field line radius and the eigenfunction (which is related to the perturbed electrostatic potential and may therefore be considered proportional to the perturbed displacement).

Details of the general high m-number stability properties of the standard multiple mirror fields have been studied by calculating the variation of ω^2 with radius, azimuth and the direction of the wave front normal. It was found (as with tandem mirrors) that the least stable fieldlines lie in the symmetry planes along the ellipse axes (where the lines possess no torsion), and near the plasma surface (at the position of the peak radial pressure gradient). The most unstable mode has displacement perpendicular to the plasma surface (and so is driven only by the normal curvature). These conditions are applied in comparing the theoretical predictions to the experimental results.

The experimental plasma is found to be more stable than predicted by flute theory. Several of the configurations to be discussed below, which are experimentally found to be flute stable, do not satisfy the $\int d\ell/B$ criteria for stability, with the integration region taken over the part of the machine bounded by magnetic mirrors T_0 and T_5 . The high m-number modes would, of course, be expected to be stabilized by FLR effects. The low m-number modes, and particularly the $m = 1$ mode, are not FLR stabilized. However, the existence of long solenoidal regions on each side of the multiple mirror device, which contain fairly high β

plasma during the experimental times, would substantially lower the growth rate of these modes. Thus a ballooning mode may be essentially line-tied to the sizeable inertia of the solenoidal plasma regions.

In all of the numerical calculations the interaction region that was examined extended over only that part of the device bounded by the left and right final mirror throats. In order to account for the difference between this configuration and the experimental one, two theoretical ballooning calculations were performed. In the first, the mode amplitude was assumed free at the boundaries, and ballooning noted by the ratio of the mode amplitudes between the unstable and stable regions. It was considered that for ballooning to be important, a significant difference in mode amplitude should exist between these points. Somewhat arbitrarily the criterion for ballooning was taken as a mode amplitude ratio of 1.5, which was also considered to be the smallest mode amplitude ratio that was experimentally observable. For these boundary conditions the mode is generally flute unstable, and the transition to ballooning could therefore not be signaled by a change in the sign of ω^2 as β is increased. In the second calculation the mode amplitude was arbitrarily fixed to zero in the bounding mirror throats and a value of $\beta = \beta_c$ determined for which $\omega^2 = 0$. This over-restrictive boundary condition would be expected to give a value of β_c which bounds the experimentally determined β_c from above.

The experimental mode shape would be expected to lie between the mode shapes of these two model problems, and the ratio of the amplitudes between the unstable and the stable cases would be expected to be greater than 1.5 for a critical β of the order of that found for the free boundary case. These mode shapes are illustrated in Fig. 14 using a typical experimental configuration. The theoretically computed free and

fixed boundary modes are given, together with an artists conception of the expected experimental mode shape. It is interesting to note that the mode amplitude changes quite sharply at the position of easy bending.

Due to the line-tying in the experiment, the value of the β for an observed amplitude ratio of 1.5, will be lower than the value determined by the free boundary theory. This was generally found to be the case; i.e., both the free and fixed boundary condition theories provided upper bounds on the experimentally determined critical β 's. However, in the experiment there was considerable shot to shot variability. The experimental criterion used was that an amplitude ratio of at least 1.5 be consistently observed. Thus for most shots the amplitude ratio was generally greater than 1.5. Therefore, the upper bound from the free boundary condition model turned out to be quite close to the experimental observations.

The four field configurations that were investigated experimentally with the counterstreaming source plasmas were also investigated numerically. As with the experiment, for each configuration various mirror ratios and quadrupole strengths were employed, to explore a range of drive and connection length parameters. Schematics of the flux surfaces and representative axial plots of the fieldlines and eigenfunctions are given in Fig. 15, for the three unstable configurations corresponding to the experimental cases (ii) through (iv). The eigenfunctions shown in the figure are calculated with free end boundary conditions, the plasma radius is taken to be 2 cm and the integration is carried out along a fieldline, indicated as the solid line on the flux surface schematics, in the symmetry plane which lies at 1.5 cm radius in the stable cell midplanes. The values of β were chosen in each case to make the ratio of the maximum to minimum mode amplitude equal to 1.5.

In the following discussion, the theoretical results for each of the four cases studied experimentally are given. For all but case (i), both free and fixed boundary conditions are employed.

Case (i): With the multiple mirror fields that are theoretically stable to flutes at low β (MAFCO) the MHD ballooning code predicts stability at all values of β up to and beyond the validity of the code. With smaller weak quadrupole currents the ballooning code predicts instability at essentially the same value of the stabilizing currents as predicted by MAFCO, for all values of β . There is no significant mode amplitude ratio between stable and unstable regions at any β , indicating that finite β ballooning effects are not important for this configuration (short connection lengths and no adjacent easy bending region). The experiment is more stable than the theoretical predictions (for flutes) as described in Section III.

Case (ii): The weakly unstable region shown in Fig. 15a, which is two cells in length, is created by removing all quadrupole and mirror currents (leaving only a solenoid) between M_{12} and M_{34} . This configuration is very similar to the tandem mirror. In the stable cells the mirror ratio is 3, and the quadrupole fields are reduced slightly to produce a maximum ellipticity of 10. Since the destabilizing curvature is weak and mainly occurs near the bounding good curvature mirror throats the critical beta is expected to be relatively high. In the experiment the plasma was observed to balloon at and above $\beta \approx 15$ percent. The free boundary mode calculation predicts an amplitude ratio of 1.5 at $\beta = 22$ percent. The eigenfunction in Fig. 15a indicates that the fieldline bending is abrupt through the left transition (near $z = 75$) for which the fieldline is "soft" (lying along an ellipse minor axis). The amplitude then decays in a nearly linear fashion through the "stiff"

transition at the right boundary. The symmetry of the configuration is such that the 90° fieldline, (shown dotted in Fig. 1a) exhibits the same amplitude profile with "soft" and "stiff" transitions reversed. If the mode amplitude at the end points is clamped to zero, then the theory predicts a $\beta_c = 40$ percent. This is clearly well above the experimental value, but this is an upper bound result.

Case (iii): Both the drive, and the connection length to the regions of strongest drive, are increased by introducing two mirrors into the solenoidal region of case (ii). The flux surface, field line and eigenfunction are shown in Fig. 15b.

Experimentally, for moderate drive ($M=3$) ballooning activity was observed to be initiated at $\beta \approx 10$ percent. The free end calculation shown in Fig. 1b indicated ballooning (a mode amplitude ratio of 1.5) at $\beta = 10$ percent. For both ends fixed with the same code $\beta_c \approx 15$ percent. For stronger drive ($M=4$) the experimentally observed $\beta_c \approx 5$ percent. This is to be compared with the free end value of $\beta_c = 7$ percent for ballooning and the fixed end $\beta_c = 11$ percent.

Case (iv): In the fourth configuration the experimental fields were pulsed into a configuration identical to that in which the preliminary single source results were obtained with steady state fields (see Fig. 6). In this configuration the weak quadrupoles between T_1 and T_3 were set to zero. In the absence of the quadrupole component the fieldlines do not "recircularize" at the midplanes in the unstable zone, so that the entire region is nonaxisymmetric. The symmetry between the 0° and 90° fieldlines is broken and this fact makes the analysis of this configuration quite complicated. Specifically the 90° fieldline is strongly unstable and the free end calculation (for $M=4$ and the full optimal quadrupole current) predicts ballooning onset at $\beta_c = 2$ percent.

The corresponding fixed end calculation predicts a $\beta_c = 5$ percent. The 0° fieldline possesses very little negative curvature and is quite stable to ballooning. The free end calculation along this line predicts flute stability, with a beta value for marginal stability ($\omega^2=0$) of $\beta = 40\%$. The corresponding fixed end case is stable to ballooning up to $\beta = 1$.

Experimentally no ballooning activity was observed for weak drive (mirror ratio $M = 3$) up to the highest observable β 's ~ 25 percent. For stronger drive ($M=4$) ballooning is observed for $\beta_c \geq 10$ percent and for very strong drive ($M=5$) ballooning occurred for $\beta_c \geq 7.5$ percent. The reduced data previously shown in Fig. 10 of section III is for the strong drive ($M=5$) experiment. Note that, consistent with the theory, the displacement is chiefly along a direction lying in the 90° symmetry plane. Since the observed mode is primarily $m = 1$, which averages over azimuthal angles, the experimentally observed β_c is expected to be higher than the high m -number theoretical result for β_c on the most unstable field line.

In summary, the results of the one stable and three unstable cases are given in Table 1. As expected the fixed end point theoretical calculations bound the experimental β_c from above, except in configuration (iv) for which some azimuthal weighting is required. The criterion that a ratio of mode amplitudes of 1.5 be present in the theory with free ends appears to be a reasonable predictor of the value of β at which ballooning was experimentally observed.

REFERENCES

1. M. Tuszewski, D. Price, M.A. Lieberman, R. Bravenec, K. Doniger, and C. Hartman, "MHD-Stabilization of Finite- β Multiple-Mirror Plasmas," Nucl. Fusion 19 1243, (1979).
2. H.P. Furth, J. Killeen, M.N. Rosenbluth and B. Coppi, "Stabilization by Shear and Negative V," Plasma Physics and Controlled Nuclear Fusion Research, Vol. 1, (1965).
3. T.B. Kaiser, "Numerical Investigation of the Ballooning Stability of TMX at Finite β " Bull. Am. Phys. Soc. 23, 754 (1978).
4. T.B. Kaiser, L.D. Pearlstein, "Ballooning Modes in Quadrupole Tandem Mirrors," Lawrence Livermore National Laboratory Report, UCRL-87659, (1982)
5. J.C. Riordan, A.J. Lichtenberg, M.A. Lieberman, "Minimum-Average-B Wells in Linked Magnetic Mirror Fields," Nucl. Fusion 19 21 (1979)
6. R. Bravenec, A.J. Lichtenberg, and M.A. Lieberman, "Axial Plasma Injection and Shock Formation in Multiple Mirrors," Phys. Fluids, to be published.
7. D. Price, R. Bravenec, K. Doniger, C. Hartman, A. Lichtenberg, M.A. Lieberman, D. McColl, and M. Tuszewski, "Experimental Study of Plasma Confinement in the Ten Meter Multiple Mirror," Bull. APS 24 1056 (1979).

8. W.A. Perkins, J.C. Brown, "MAFCO - A Magnetic Field Code for Handling General Current Elements in Three Dimensions," Lawrence Livermore National Laboratory Report, UCRL-7744-Rev II (1966).
9. W.A. Newcomb, "Large-Aspect-Ratio Equilibrium and Stability," Lawrence Livermore National Laboratory Report UCID-17182 (1976).
10. M. Tuszewski and A.J. Lichtenberg, "Two Dimensional Boundary Value Problem for Ion-Ion Diffusion," Phys. Fluids 20 1263 (1977).

Table 1

Summary of Configurations, Experimental and Theoretical β_c (percent)

Configuration Description	$\beta(\text{exp.})$	$\beta(\text{theory})$	
		Free	Fixed
(i) Standard fields	stable ($\beta > 25\%$)	100	
(ii) No quadrupole from $M_{12} - M_{34}$ T_2 and T_3 off; reduced quad.	15	22	40
(iii) Pulsed off WQ from $M_{12} - M_{34}$			
(a) $M = 3$; reduced quads	>10	10	15
(b) $M = 4$; full quads	>5	7	11
(iv) Pulsed off WQ from $T_1 - T_3$			
(a) $M = 4$; full quads			
$\theta = 90^\circ$	>10	2	5
$\theta = 0^\circ$		40	100

FIGURE CAPTIONS

- Fig. 1. Schematic of the multiple-mirror experiment, axial magnetic fields and plasma sources. Only part of the device is shown (note break near right end). The quadruple coils and fields are not included in the sketch.
- Fig. 2. Sketch of flux surfaces of the first two cells in the standard multiple mirror configuration, shown together with actual pictures of the flux cross sections taken with a plasma camera and using an electron beam source located in the guide field.
- Fig. 3. Schematic of the probe positions in two cells M_{23} and M_{34} for some of the instability measurements, together with the actual scope traces from the probes. The relative position of the probe tips (dots) at 1.5 cm radius with respect to the vacuum chamber of 4.3 cm radius is shown. The symbols are T (top), F (front), B (bottom), and R (rear). A plasma camera picture taken on the same shot and terminating the plasma at M_{45} is also shown. The discontinuity on the probe traces at $\sim 120 \mu\text{sec}$ indicates the time at which the plasma camera picture was taken.
- Fig. 4. Stable density decay versus time in the multiple mirror with a single (theta-pinch) source. The circled points indicate the peak β obtained in the three observation cells $M_{12}(x)$, $M_{34}(+)$ and $M_{45}(o)$. The measured values of temperature $T_i = 5\text{eV}$ and radius $r_p = 3 \text{ cm}$ are used for the theoretical calculations. The upper dashed curve assumes electron-ion collisions only, valid at short mean free paths (higher density) when the losses in the fans are unimportant. The lower dashed curve includes

the higher order classical ion-ion collisions in the fans, which are important at longer mean free paths (lower density). (10)

- Fig. 5. The experimental centroid (\bar{x}) of the unstable plasma is shown as a function of time, as calculated from the probe traces also shown. The circles about each centroid indicate the uncertainty in determination of the centroids. The mode amplitude is seen to be rotated by 45° between adjacent cells, which may be due to a combination of radial fields and partial line tying. Circles (in all figures) indicate vacuum chamber.
- Fig. 6. The centroid of the plasma versus time, shown for local destabilization (no weak quadrupoles) in cells two and three. The mode, which is growing as it convects axially through the unstable cells two and three, partially restabilizes in cell four. The flux surface for this configuration is also shown.
- Fig. 7. Mode number identification on three different shots. The general features of the mode can be discerned from the probe traces, including the plasma centroid. The discontinuity in the probe traces corresponds to the time of taking the plasma camera picture.
- Fig. 8. Values of β in three of the first four midplanes obtained from diamagnetic loops with time as a parameter. The dashed extrapolations to cell five are consistent with data from Langmuir probes with $T_i = T_e = 15\text{eV}$.

- Fig. 9. Stable decay in the multiple-mirror configuration ($M = 5$).
Langmuir probe tips are (in all figures) at a radius of 1 cm.
- Fig. 10. Globally destabilized plasma motion (flute) obtained by removing weak quadrupole fields ($M = 5$).
- Fig. 11. Locally weakly destabilized plasma, obtained by removing all mirror and quadrupole fields from two cells. (a) flux surface; (b) plasma motion.
- Fig. 12. Locally strongly destabilized plasma, obtained by pulsing on two magnetic mirrors in the configuration of Fig. 11. (a) flux surface; (b) plasma motion.
- Fig. 13. Locally destabilized plasma with strong azimuthal asymmetry. The flux surface is as shown in Fig. 6a when the weak quadrupoles are pulsed off.
- Fig. 14. Sketch showing the eigenfunctions for the two theoretical models to be compared with the expected experimental mode shape. (a) Flux surface; (b) mode shape with free boundary; (c) mode shape with fixed boundary; (d) expected experimental mode shape.
- Fig. 15. Flux surface, field line shape, and eigenfunction for: (left) case (ii) local weak destabilization; (center) case (iii) local strong destabilization; and (right) case (iv), local destabilization with strong azimuthal asymmetry.

MMX Schematic

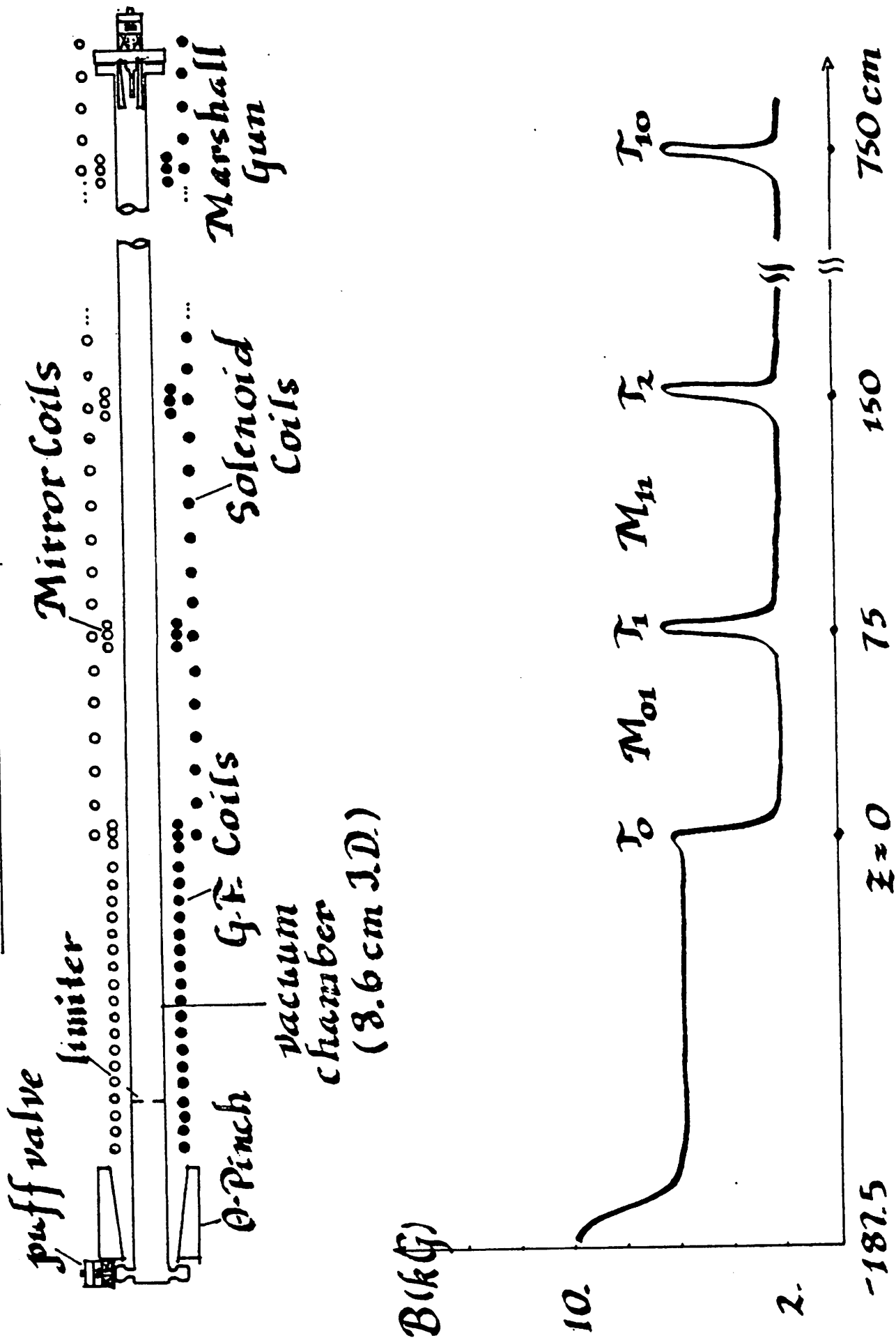
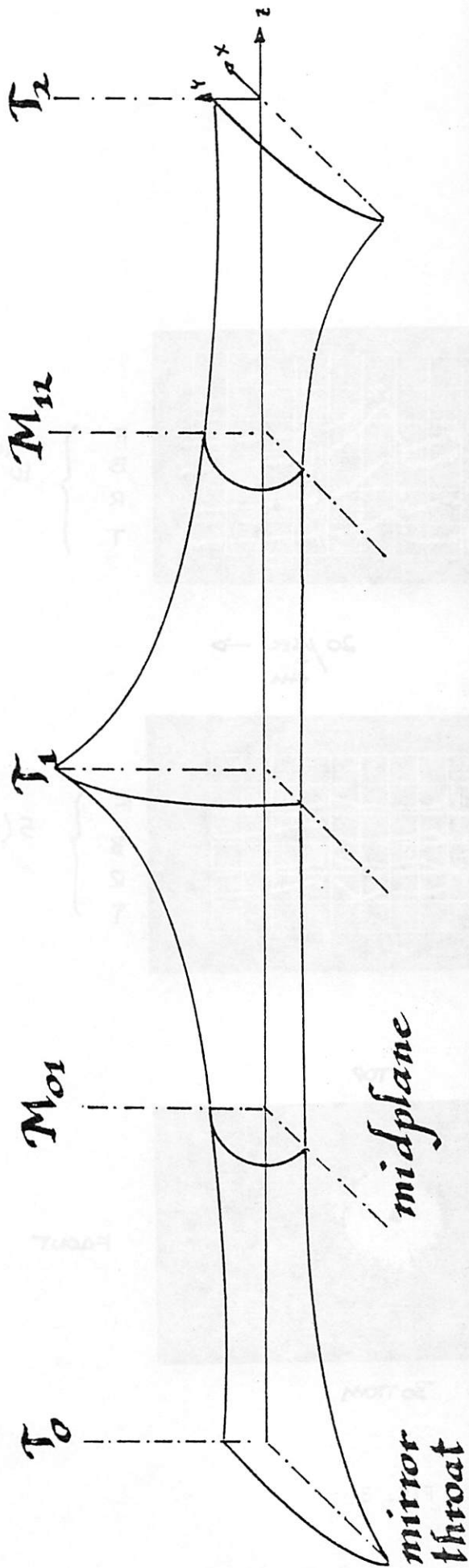
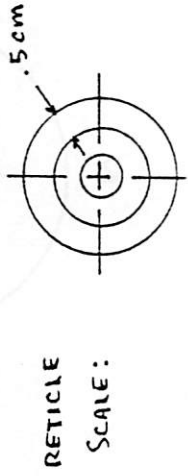


FIG. 1

Flux Surfaces

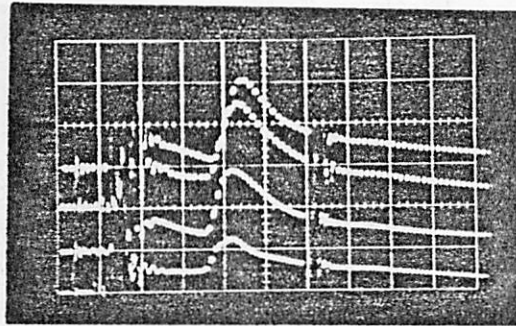
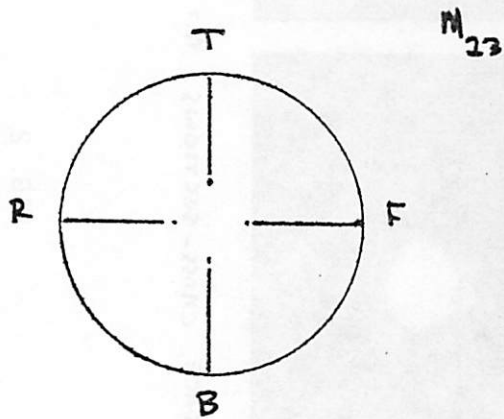


PLASMA CAMERA PICTURES OF FLUX SURFACE CROSS-SECTIONS: $M=4$, $q \sim 2.5$



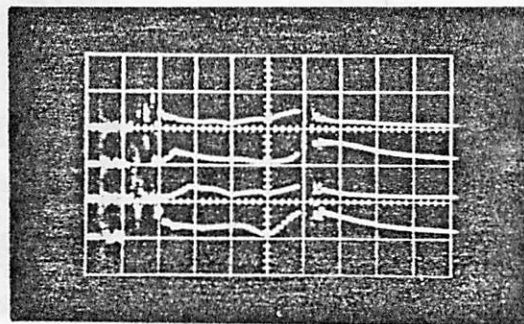
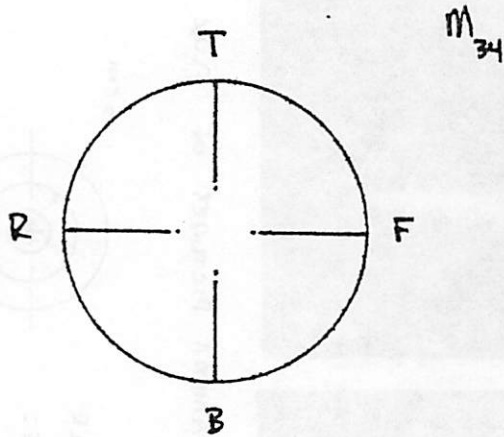
RETICLE
SCALE:

FIG. 2



F
B
R
T } $10^{14} \frac{\text{cm}^{-3}}{\text{cm}}$ ↑

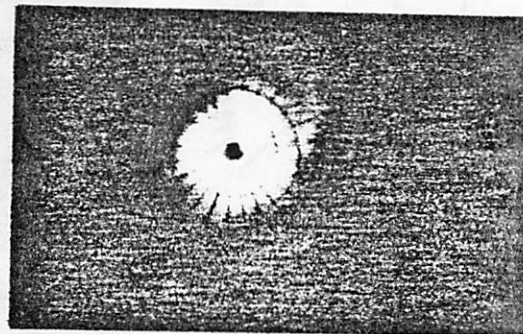
$20 \frac{\mu\text{SEC}}{\text{cm}} \rightarrow$



F
B
R
T } $5(10^{13}) \frac{\text{cm}^{-3}}{\text{cm}}$ ↑

M₄₅

REAR



TOP

BOTTOM

FRONT

FIG. 3

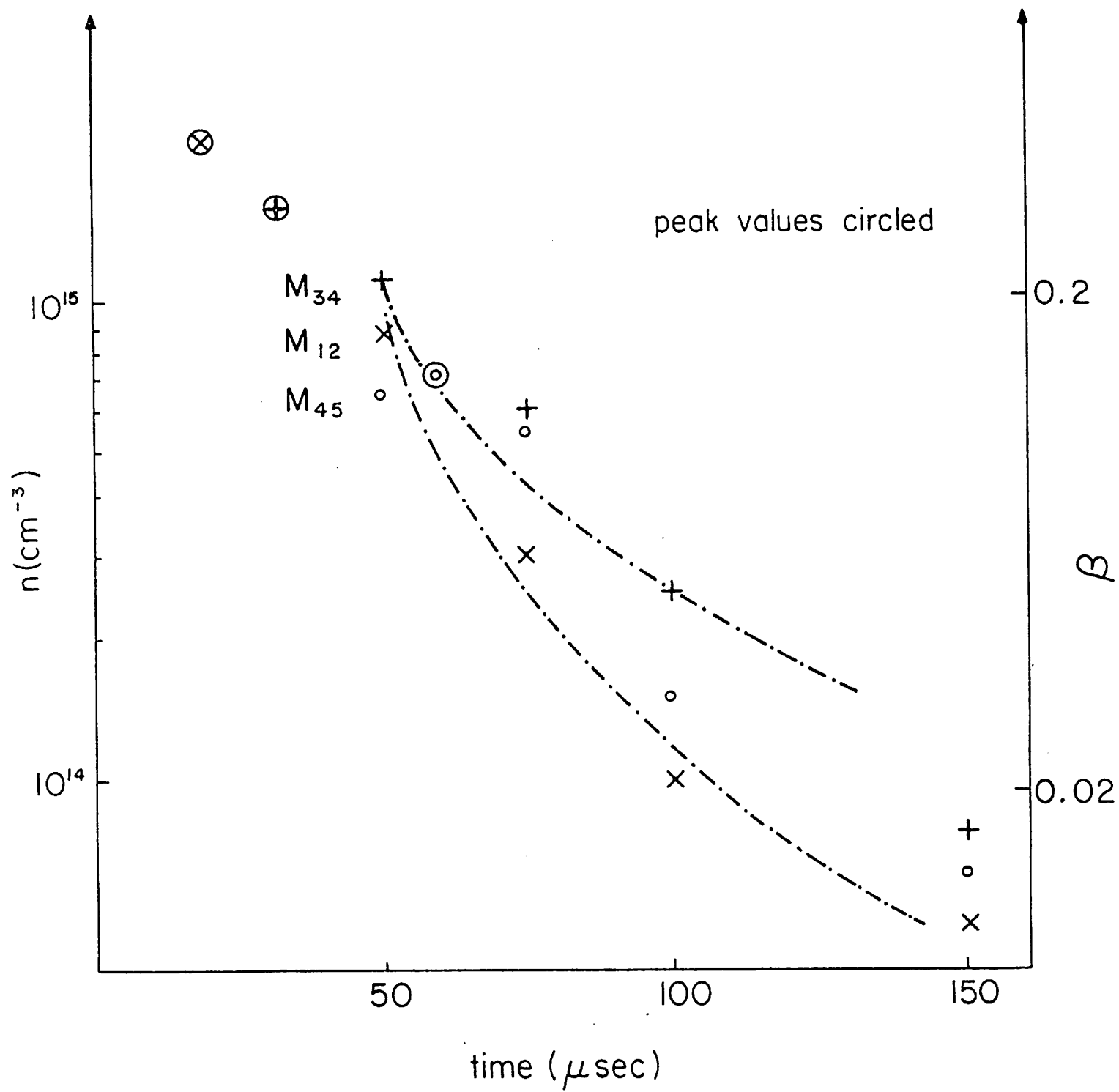


FIG. 4

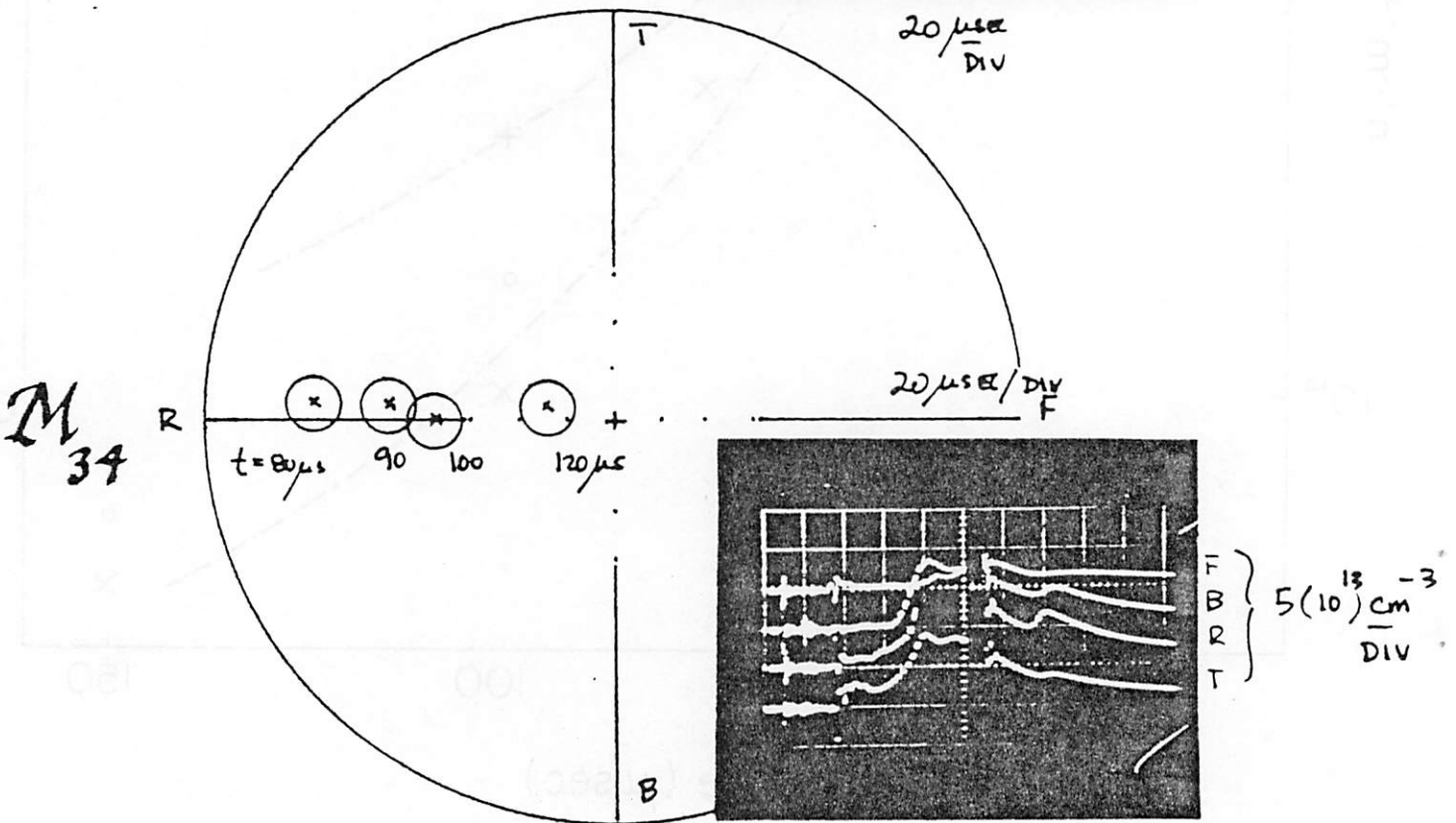
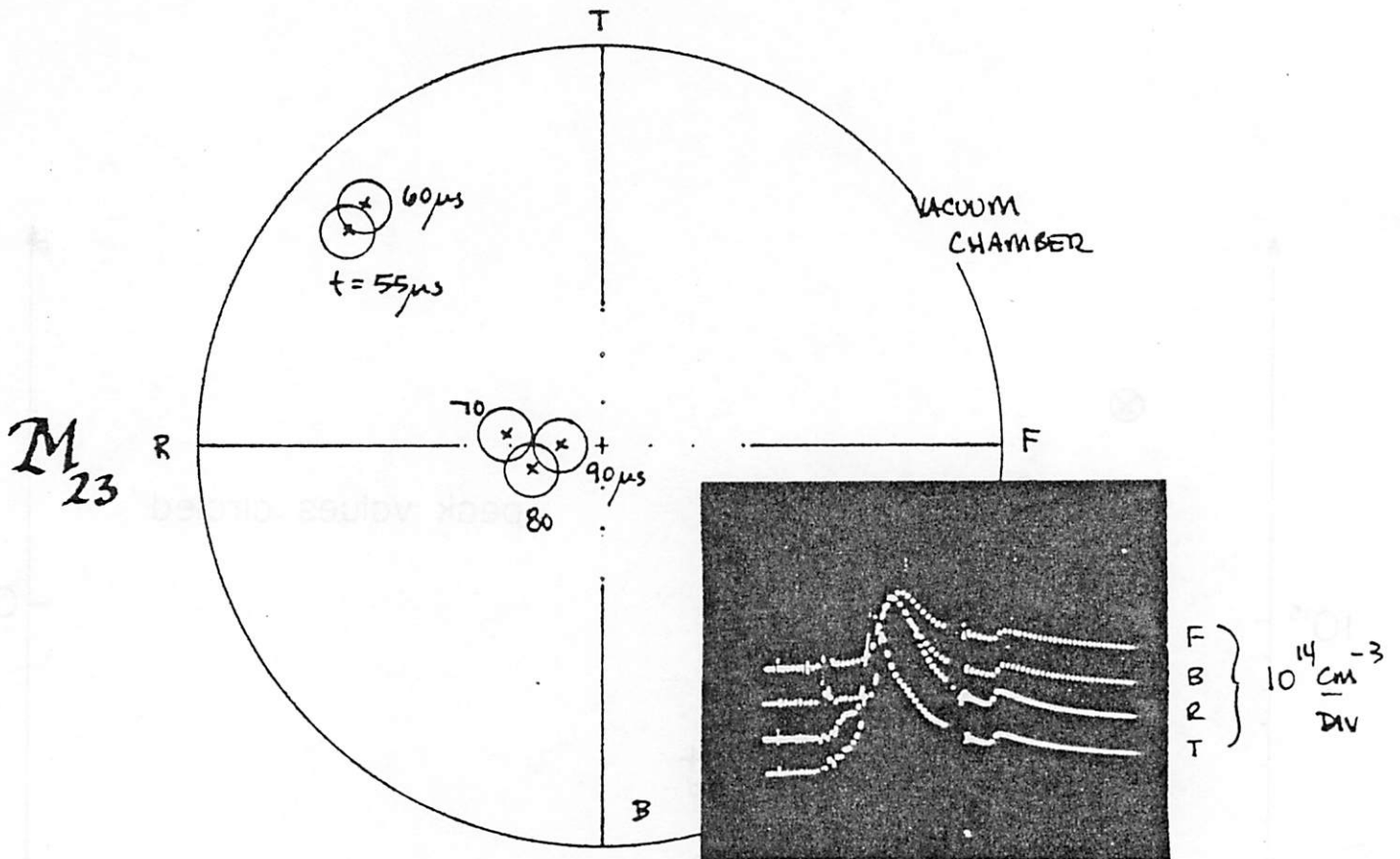


FIG. 5

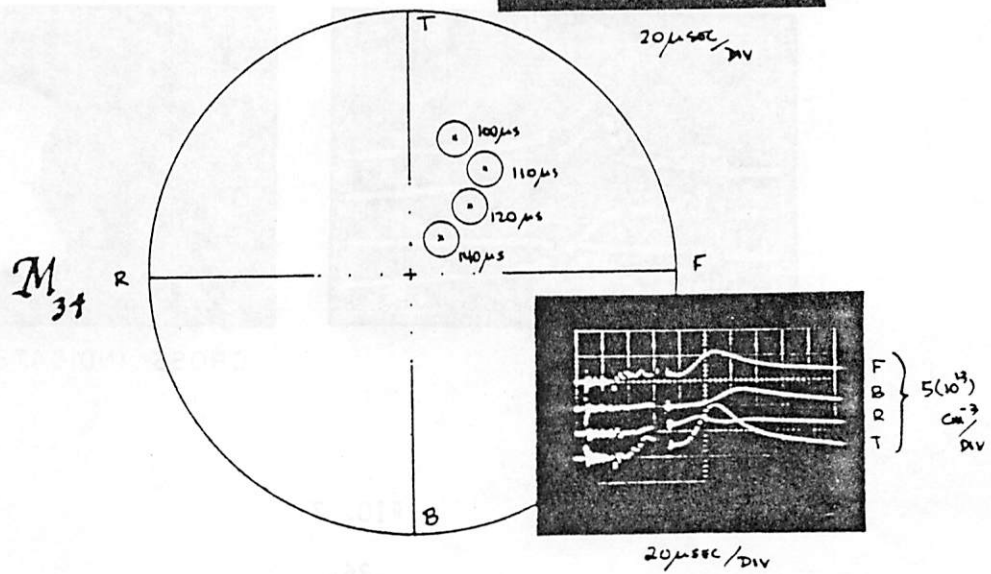
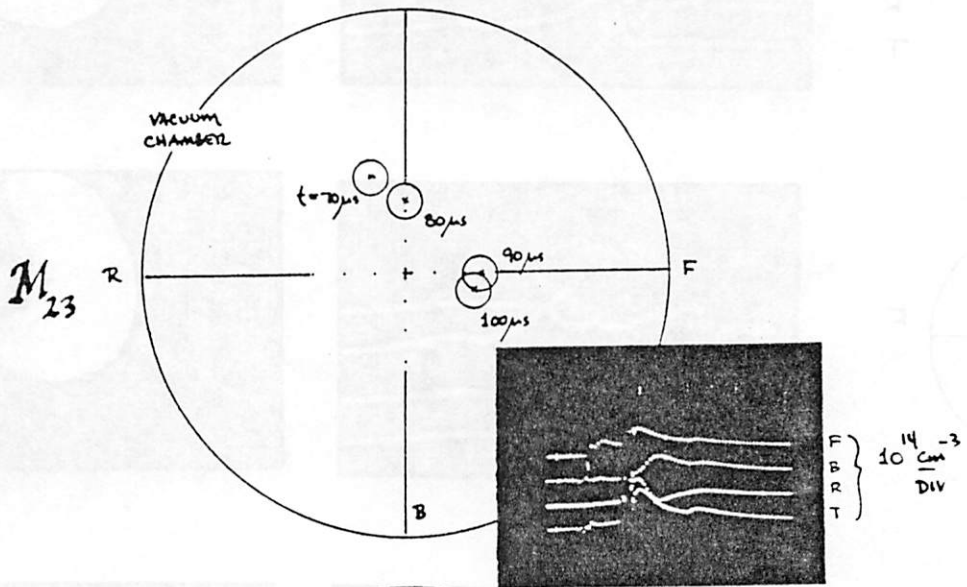
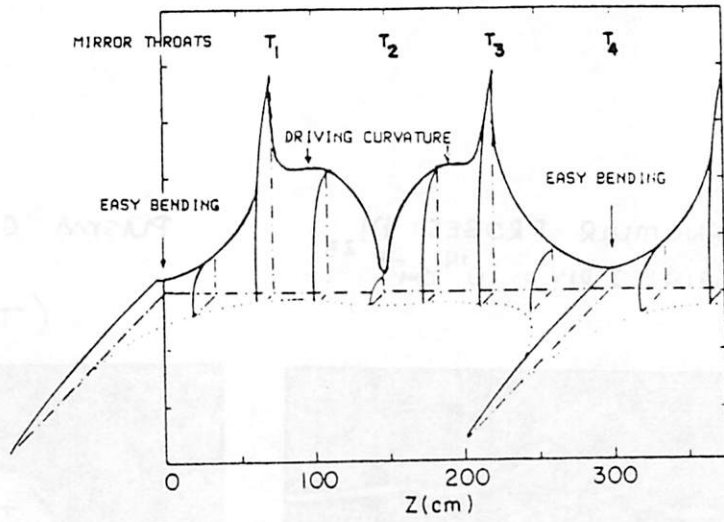


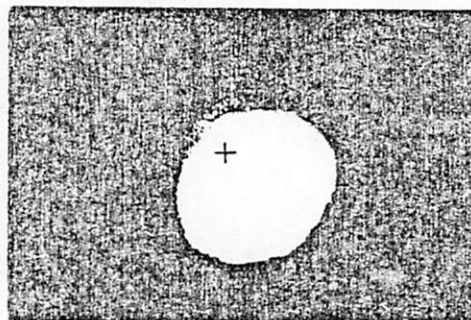
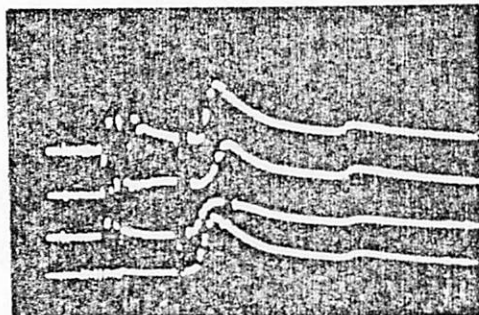
FIG. 6

LANGMUIR PROBES: M_{23}
 GAIN: 1 DIV = 10^{14} cm^{-3}

PLASMA CAMERA PHOTOS: M_{34}

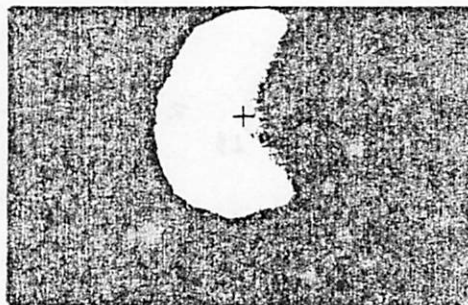
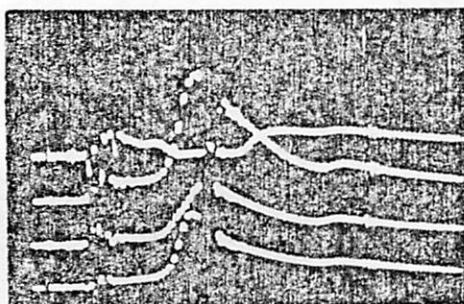
(TOP)

F
B
R
T

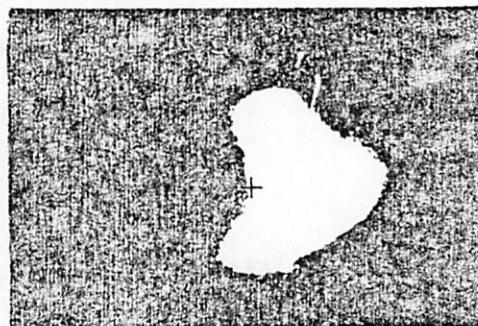
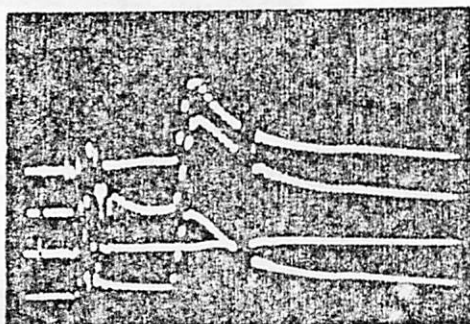


(FRONT)

$m = 1$



$m = 2$



$m = 3$

CROSS INDICATES AXIS

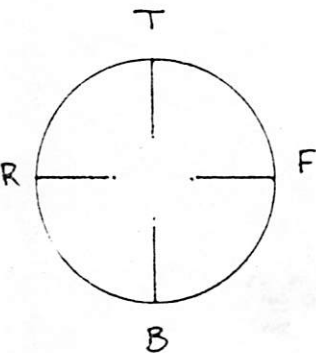


FIG. 7

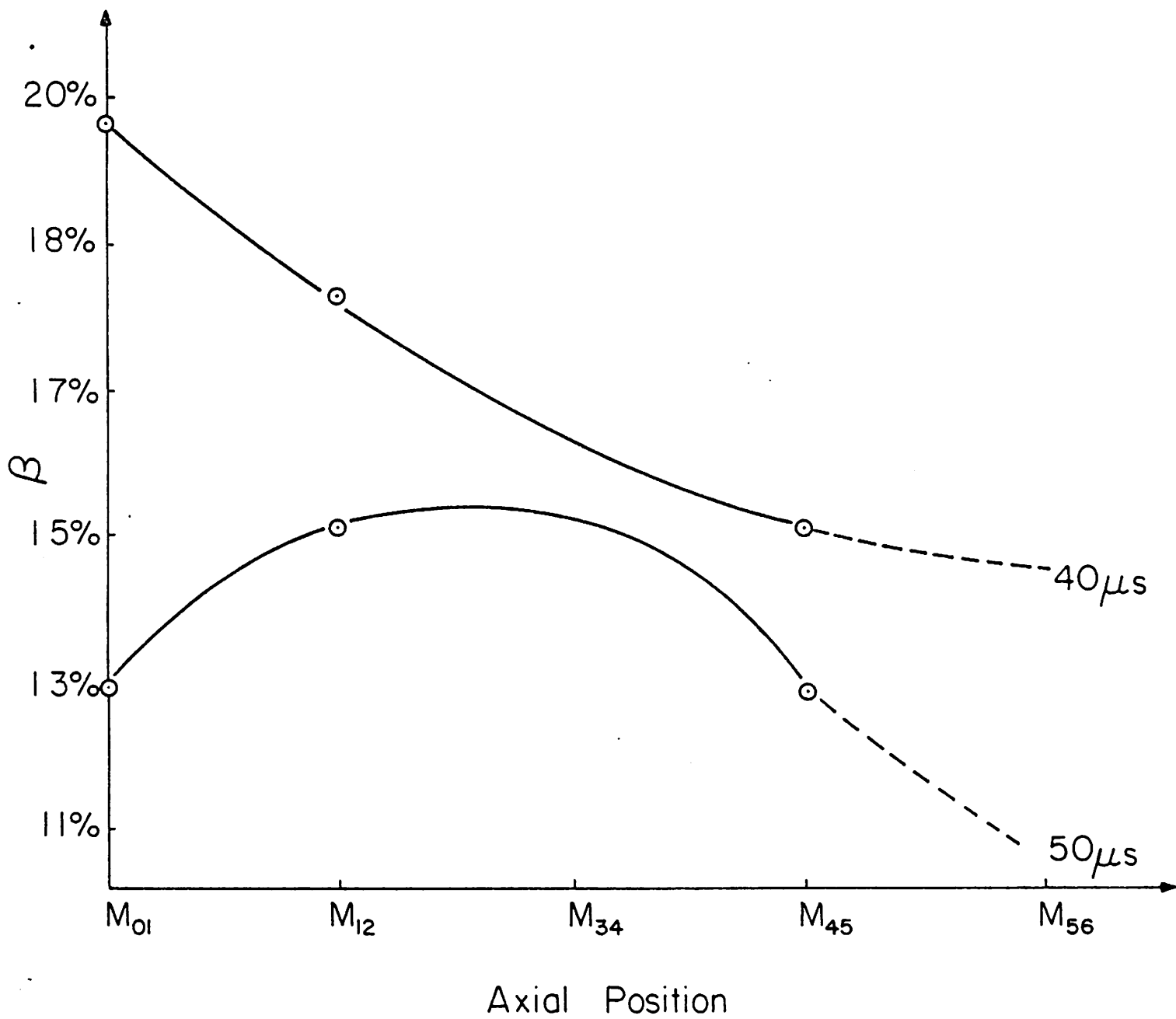
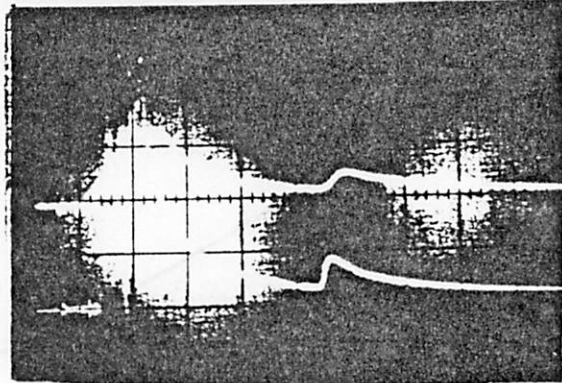
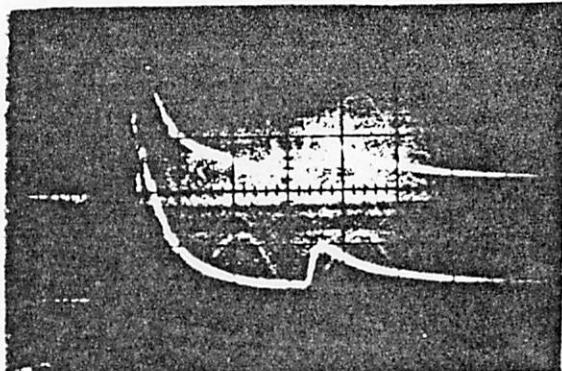
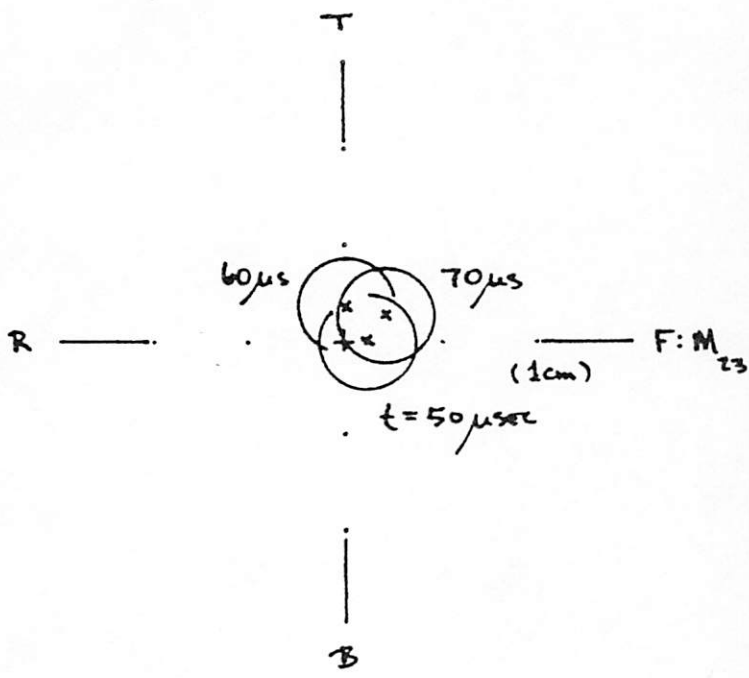
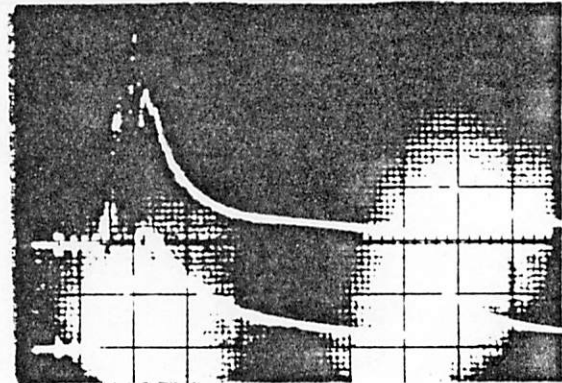
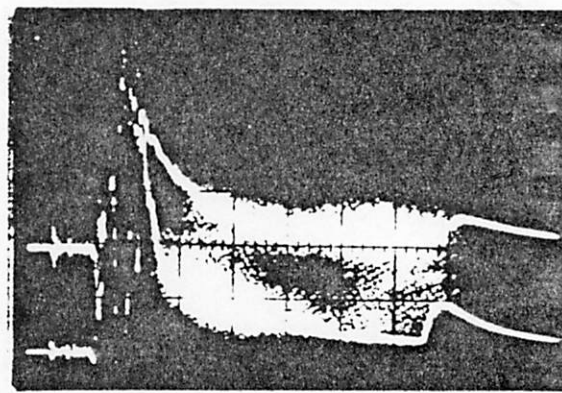
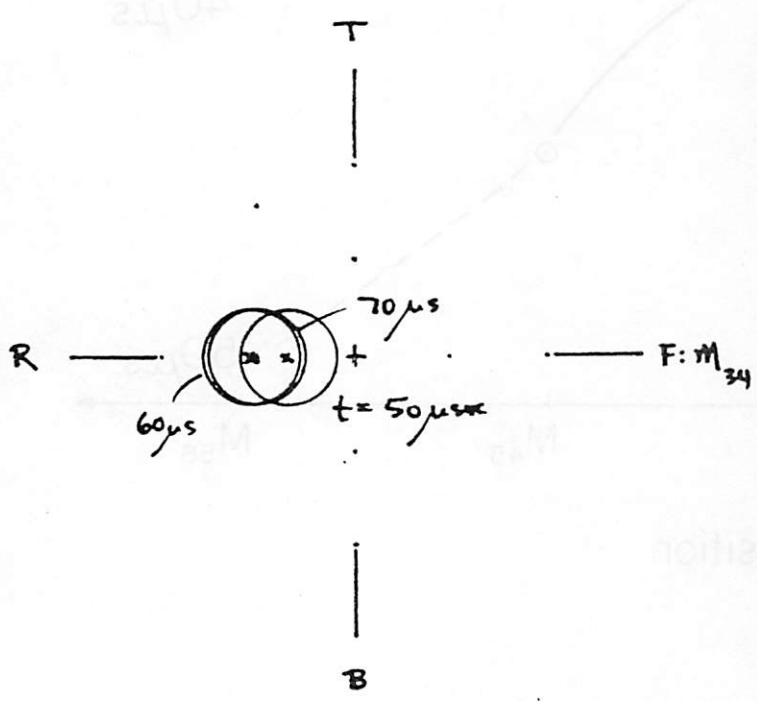


FIG. 8

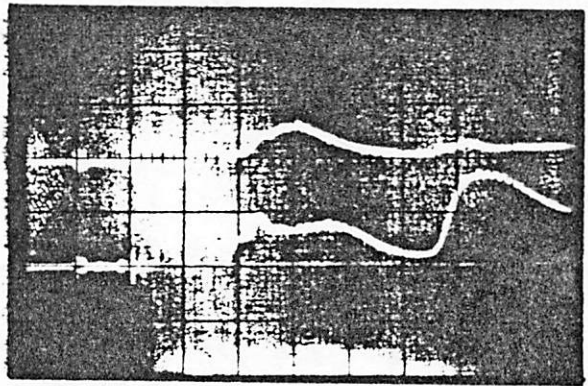
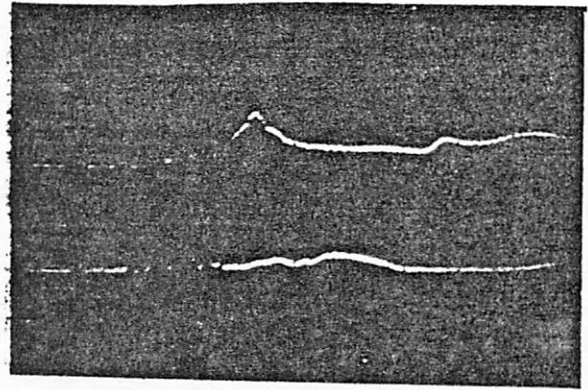
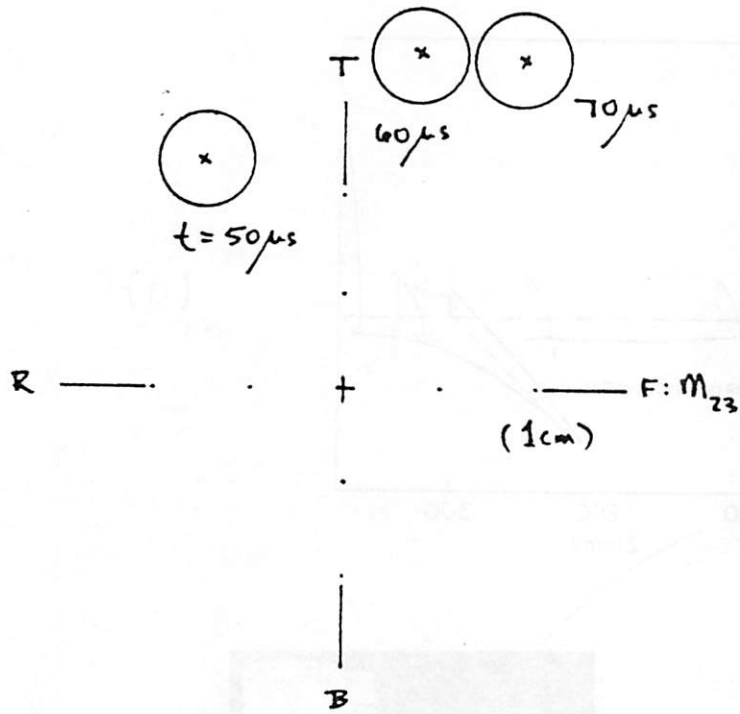


F
 B
 } $10 \frac{M^{-3}}{\text{DIV}}$
 R
 T

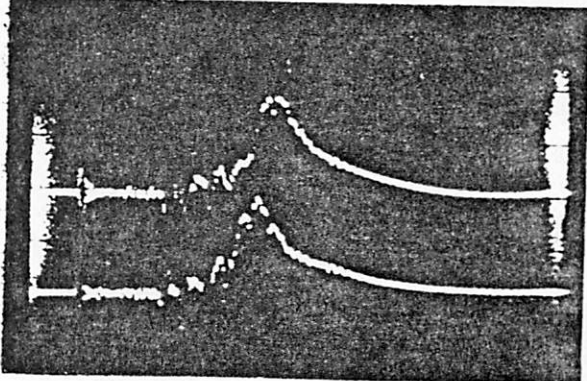
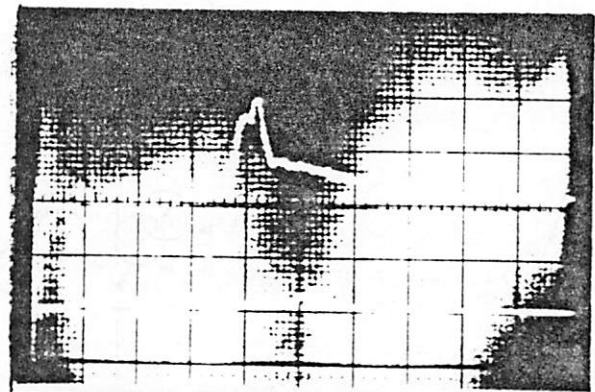
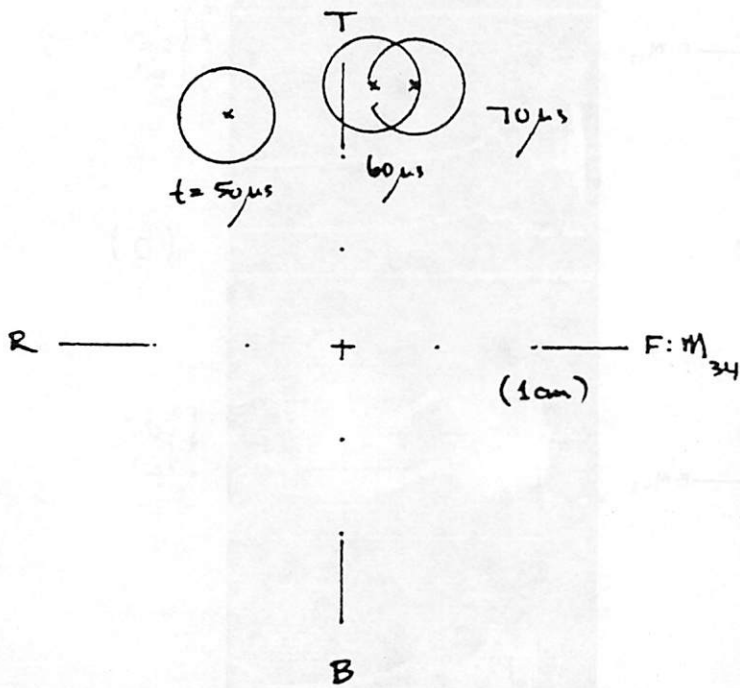


F
 B
 } $10 \frac{M^{-3}}{\text{DIV}}$
 R
 T

FIG. 9
 -38-



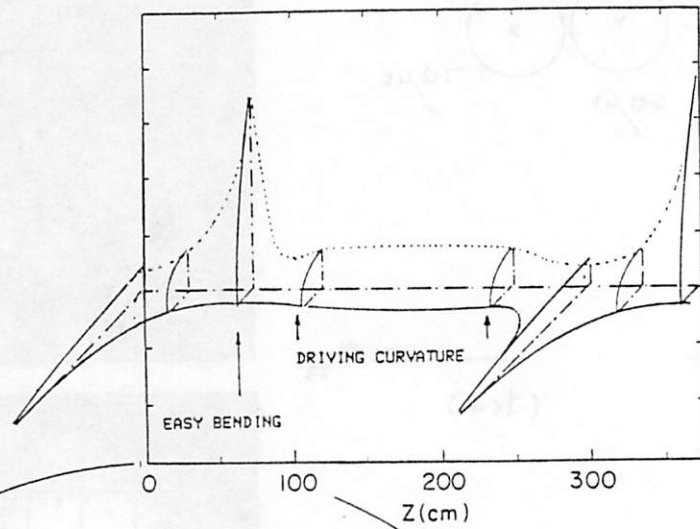
F
B
} $10 \frac{M}{cm} \text{ Div}$



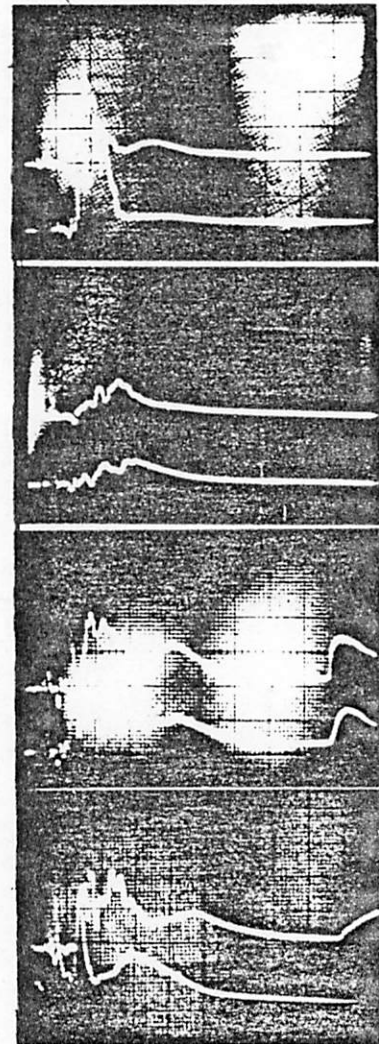
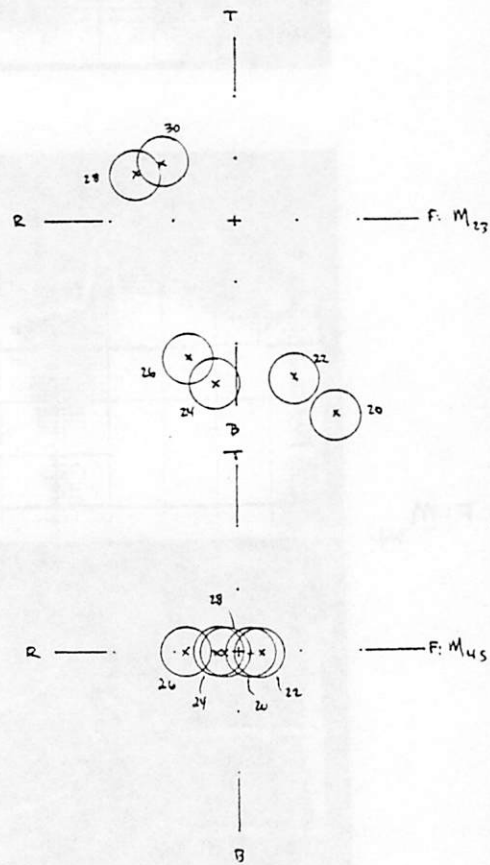
F
B
} $10 \frac{M}{cm} \text{ Div}$

$10 \frac{\mu s}{\text{Div}}$ →

FIG. 10



(a)



F } 5(10¹⁴)
B } cm⁻³
R } Div
T }

(b)

F } 5(10¹⁴)
g } cm⁻³
x } Div

Triple Probe (7eV) Div

10 μm Div

FIG. 11

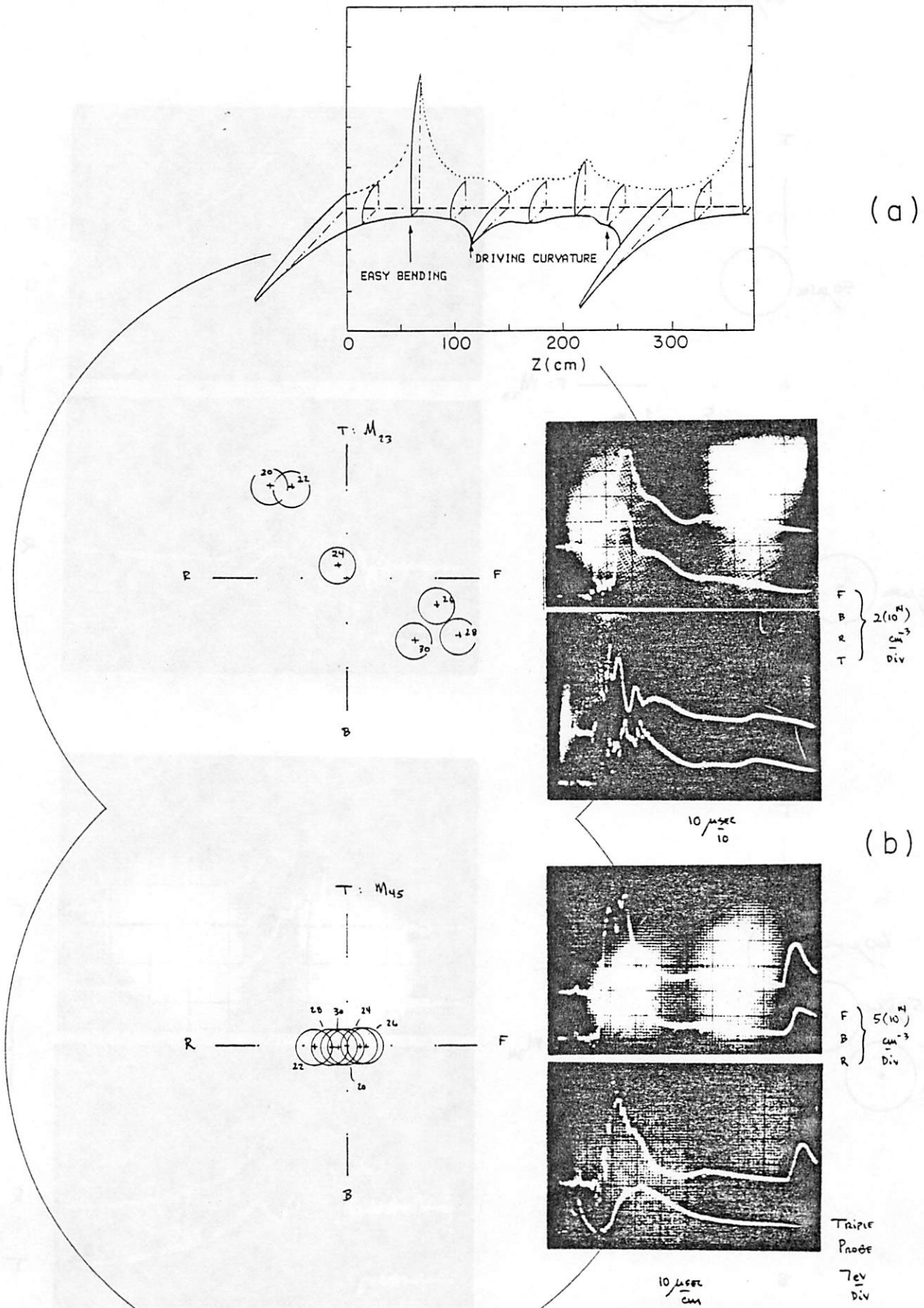


FIG. 12

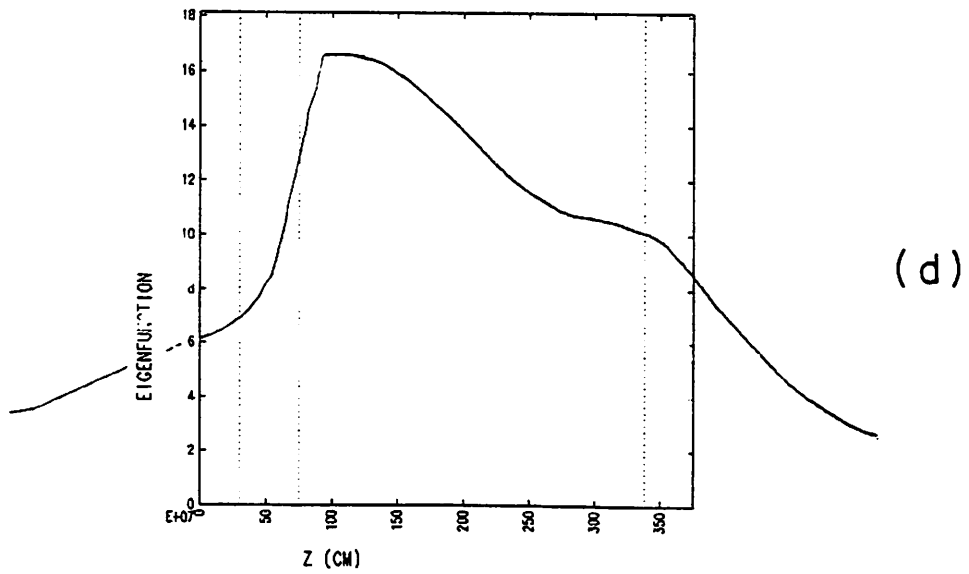
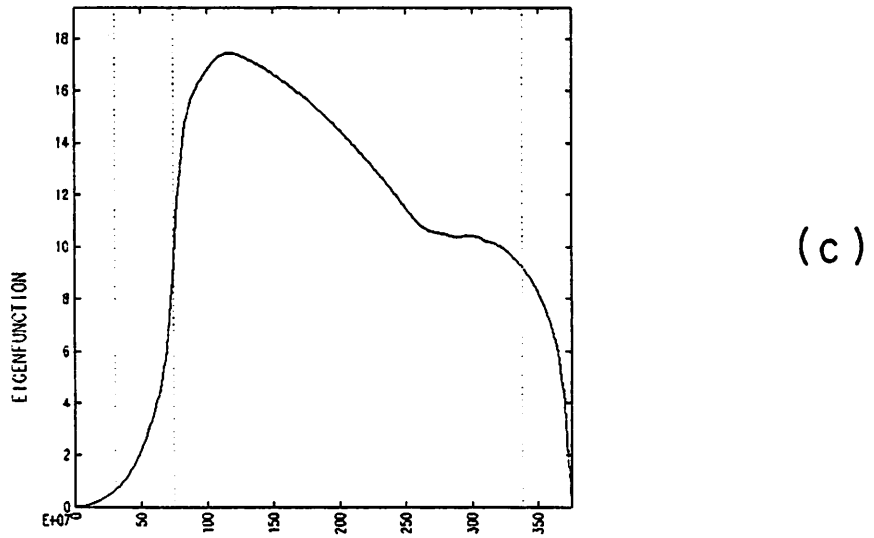
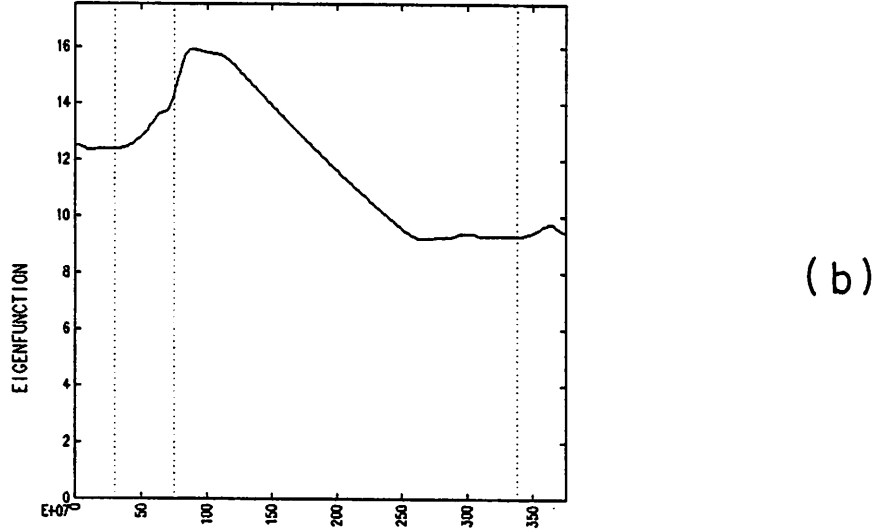
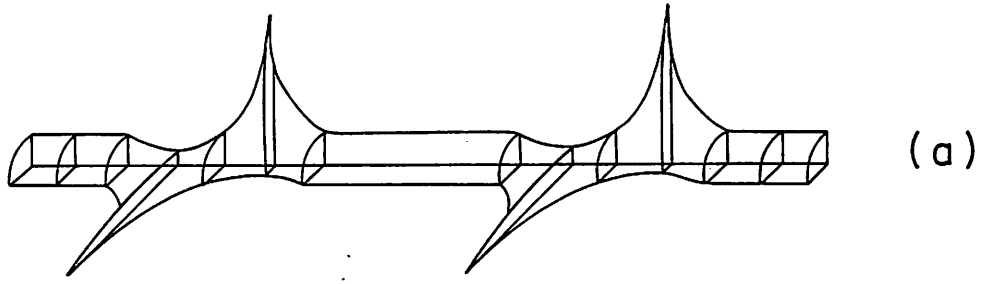


FIG. 14 -43-

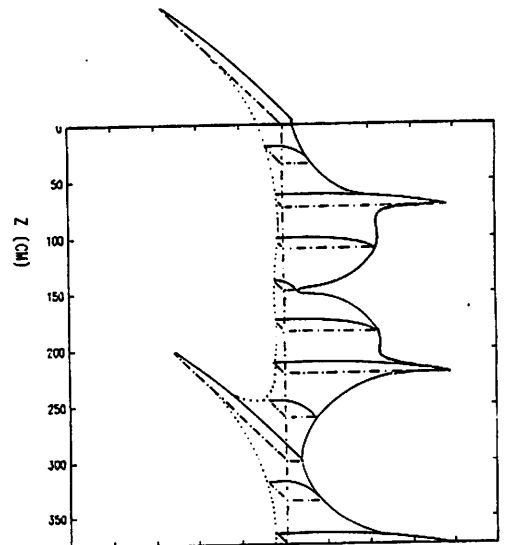
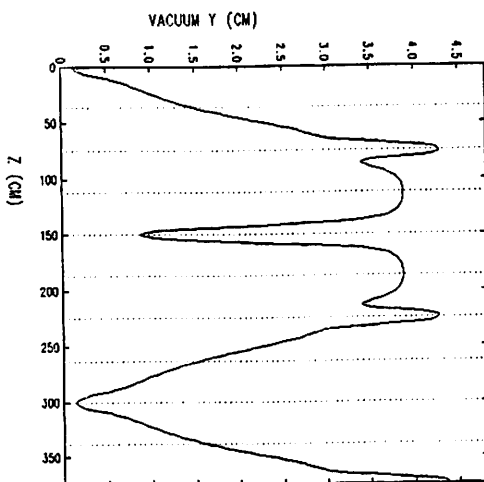
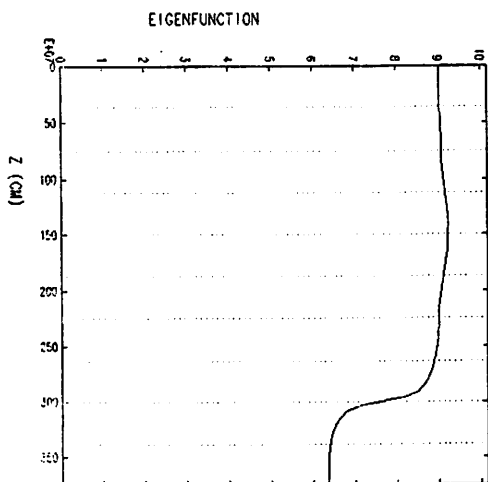
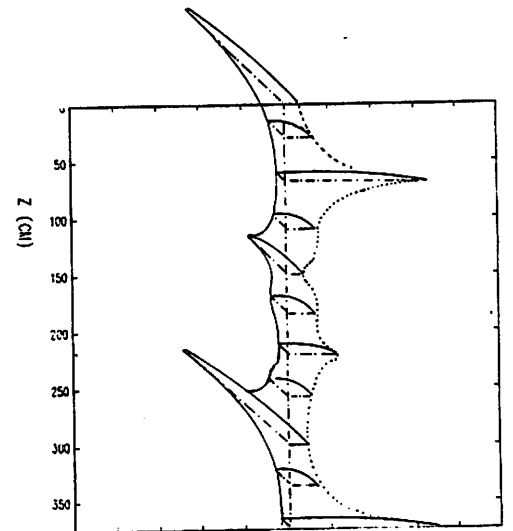
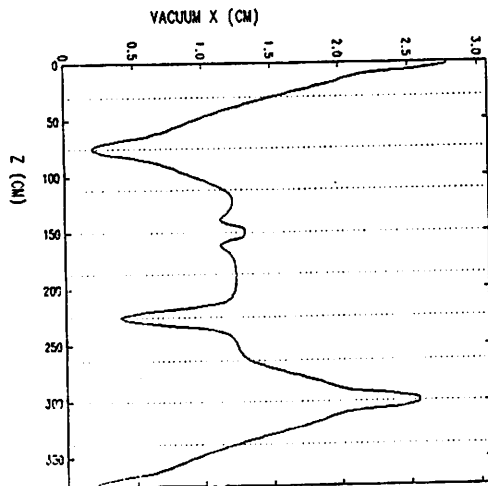
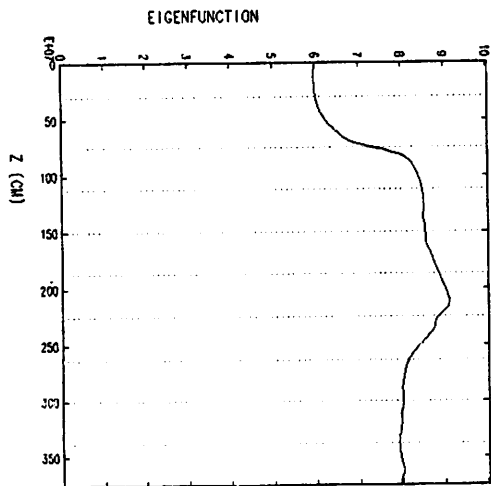
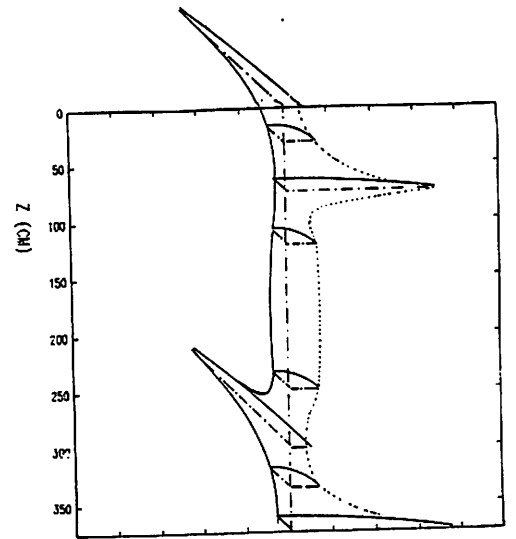
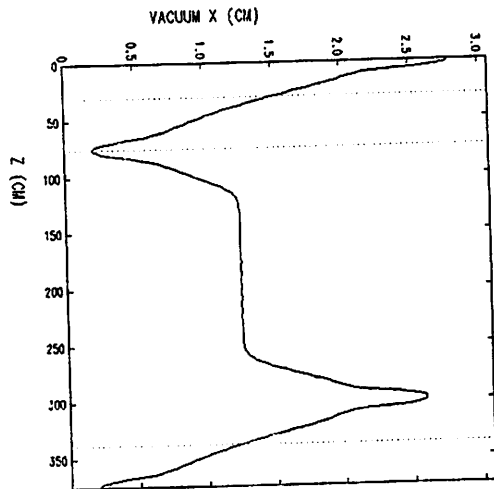
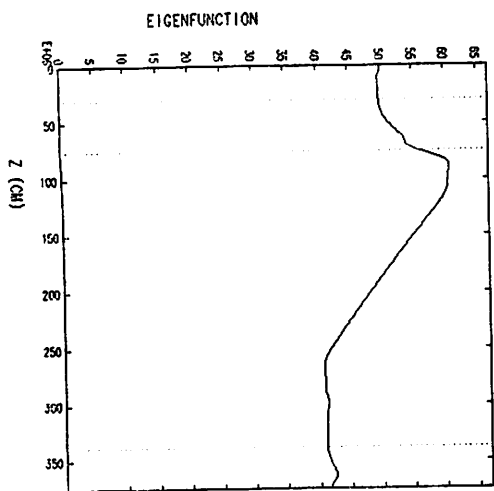


FIG. 15